Molecular Neurobiology (2025) 62:7075–7092
https://doi.org/10.1007/s12035-024-04632-4

RESEARCH

Mitochondrial Alterations in Alzheimer's Disease: Insight from the 5xFAD Mouse Model

Elif Nedret Keskinoz[1,6] · Musa Celik[2] · Ezgi Sila Toklucu[3,4] · Kerem Birisik[3,4] · Alev Erisir[4] · Devrim Oz-Arslan[2,5]

Received: 31 July 2024 / Accepted: 12 November 2024 / Published online: 11 December 2024

Abstract

Mitochondrial dysfunction is increasingly recognized as a key factor in Alzheimer's disease (AD) pathogenesis, but the precise relationship between mitochondrial dynamics and proteinopathies in AD remains unclear. This study investigates the role of mitochondrial dynamics and function in the hippocampal tissue and peripheral blood mononuclear cells (PBMCs) of 5xFAD transgenic mice, as a model of AD. The levels of mitochondrial fusion proteins OPA1 and MFN2 and fission proteins DRP1 and phospho-DRP1 (S616) at 3, 6, and 9 months of age were assessed. Western blot analysis revealed significantly lower levels of OPA1 and MFN2 in the hippocampus of 6- and 9-month-old transgenic (TG) 5xFAD mice compared to controls (CTR), while DRP1 and pDRP1 levels were increased in 9-month-old TG mice. Additionally, MFN2 were decreased in the PBMCs of 9-month-old TG mice, indicating systemic mitochondrial alterations. Ultrastructural analysis of hippocampal tissues showed substantial alterations in mitochondrial morphology, including abnormalities in size and shape, a preponderance of teardrop-shaped mitochondria, and alterations in the somatic mitochondria-ER complex. Notably, mitochondria-associated ER contact sites were more distant in TG mice, suggesting functional impairments. Flow cytometric measurements demonstrated decreased mitochondrial membrane potential and mass, along with increased superoxide production, in the PBMCs of TG mice, particularly at 9 months, highlighting compromised mitochondrial function. Levels of key mitochondrial proteins including VDAC, TOM2O, and mitophagy-related protein PINK1 levels altered in both central and peripheral tissue of TG mice. These findings suggest that mitochondrial dysfunction and altered dynamics are early events in AD development in 5xFAD mice, manifesting in both central and peripheral tissues, and support the notion that mitochondrial abnormalities are an integral component of AD pathology. These insights might lead to the development of targeted therapies that modulate mitochondrial dynamics and function to mitigate AD progression.

Keywords Mitochondrial dynamics · Western blot · Electron microscopy · MERCs · Flow cytometry

✉ Devrim Oz-Arslan
devrim.arslan@acibadem.edu.tr

[1] Department of Anatomy, School of Medicine, Acibadem Mehmet Ali Aydinlar University, Kayisdagi Cad. No. 32, Atasehir, Istanbul, Turkey

[2] Institute of Health Science, Department of Biophysics, Acibadem Mehmet Ali Aydinlar University, Kayisdagi Cad. No. 32, Atasehir, Istanbul, Turkey

[3] School of Medicine, Acibadem Mehmet Ali Aydinlar University, Kayisdagi Cad. No. 32, Atasehir, Istanbul, Turkey

[4] Department of Psychology, University of Virginia, P.O. Box 400400, Charlottesville, VA 22904, USA

[5] Department of Biophysics, School of Medicine, Acibadem Mehmet Ali Aydinlar University, Kayisdagi Cad. No. 32, Atasehir, Istanbul, Turkey

[6] Institute of Health Science, Department of Anatomy, Acibadem Mehmet Ali Aydinlar University, Kayisdagi Cad. No. 32, Atasehir, Istanbul, Turkey

Introduction

Alzheimer's disease (AD) is a complex neurodegenerative disorder primarily characterized by the accumulation of amyloid beta (Aβ) plaques and tau neurofibrillary tangles (NFTs) in the brain. These pathological hallmarks contribute to synaptic dysfunction, neuroinflammation, and cognitive decline [1, 2]. Understanding the interplay between these protein aggregates is crucial for elucidating the mechanisms underlying AD progression [3].

Among the various factors contributing to AD neuropathology, mitochondrial dysfunction has emerged as a critical player due to mitochondria's central role in oxidative stress, regulation of intracellular Ca^{2+} levels, and signaling pathways that regulate glutamate-mediated synaptic processes [4–7]. The mitochondrial dysfunction-induced intracellular Ca^{2+} imbalance can lead to synaptotoxicity and memory loss [8]. Additionally, impairments in mitochondrial quality control mechanisms such as mitophagy play a pivotal role in AD pathogenesis and subsequent cognitive decline [9]. Mitochondrial dynamics, encompassing fission and fusion processes, have been shown to be dysregulated in neurodegenerative diseases like Alzheimer's, Parkinson's, and Huntington's diseases, and this may indicate a potential link between mitochondrial dysfunction and disease progression [10, 11]. In AD,Aβ interaction with mitochondrial components and [12] morphological and ultrastructural alterations [13] suggest changes in mitochondrial dynamics [14], leading to oxidative damage, altered intracellular Ca^{2+} homeostasis,anddistruptions inAMP-activated proteinkinase mechanisms [8, 15] These processes contributeto neuronal and synaptic degeneration in AD brains [7, 10, 16–18]. Deficits in mitochondrial dynamics, including fusion and fission, may lead to fragmented mitochondria that are less efficient in energy production and more prone to generating oxidative stress. This exacerbates neuronal damage, thereby driving the progression of AD [16]. Alterations in mitochondrial dynamics are reflected in the morphological properties of mitochondria, including variations in size and shape [13, 19].

Mitochondrial dynamics refer to the tightly regulated processes of mitochondrial fusion and fission that ensure proper function, and distribution of mitochondria within a cell [20, 21]. Key proteins govern these dynamics: optic atrophy 1 (OPA1) is involved in the fusion of the inner mitochondrial membrane (IMM) while mitofusion 2 (MFN2) mediates fusion in the outer mitochondrial membrane (OMM) [22]. Fission starts with contact with the ER at OMM, and OMM-associated proteins such as mitochondrial fission 1 protein (FIS1) and mitochondrial fission factor (MFF) recruit dynamin-1-like protein (DRP1) to the constriction site [23]. Phosphorylation of Drp1 at serine 616, which is an active form of DRP-1, promotes Drp1-mediated mitochondrial fission and translocation to mitochondria. Furthermore, as signaling at the interface between the mitochondria and the endoplasmic reticulum (ER) has been implicated in neurodegenerative diseases, including AD [20], the examination of mitochondrial-endoplasmic reticulum contact sites (MERCs) in AD progression offers valuable insights into mitochondrial dynamics [24–26]. In agreement with the structural changes, disturbances in mitochondrial dynamics markers, Aβ accumulation in synaptosomal mitochondria, and mitophagy have been observed in transgenic AD mouse models, including 5xFAD, FAD, and APP [27–29]. In particular, the studies highlighting the dysregulation of key mitochondrial fission and fusion proteins, including OPA1, MFN2, and DRP1, have demonstrated significant disruptions in mitochondrial dynamics that may contribute to disease progression [30]. However, the time-dependent progression of the changes in mitochondrial dynamics markers in transgenic AD models that display hallmark pathologies of AD, such asamyloid plaques and cellular degeneration, has awaited further exploration. Moreover, while mitochondrial dysfunction is common in the brain tissue ofAD recent studies have revealed alterations in mitochondrial functions of peripheral mononuclear blood cells (PMBCs) [31]. As peripheral changes may constitute an early and easily accessible marker for the concurrent neuropathogenesis of AD, examining the correlative alterations in the blood and brain may reveal interventive insights [32–34].

To address these gaps, we investigated the role of mitochondrial dynamics in the progression of neuropathology in the well-characterized 5xFAD model of AD [35]. Specificially, we examined key regulators of mitochondrial dynamics, including proteins involved in mitochondrial fusion and fission, as well as the ultrastructural correlations of altered mitochondrial function in the hippocampus. Additionally, we evaluated the mitochondrial function of PMBCs in the same animals. Our research revealed that the 5xFAD mouse model's brain and peripheral tissue had considerable changes in mitochondrial dynamics.

Materials and Methods

Animals and Housing

The 5xFAD mouse line, harboring five familial mutations of FH-related genes, along with the genetic backgrounds of C57Bl/6 and SJL (strain: B6SJL-Tg), was obtained from Jackson Laboratory (MMRRC_034840-JAX and stock no. 034848-JAX) in Bar Harbor, ME, USA. These mice have a mixed genetic background of C57Bl/6 and SJL (strain: B6SJL-Tg). The mice were bred and raised at the Acibadem Mehmet Ali Aydinlar University Laboratory Animal Application and Research Center (DEHAM, Istanbul, Turkey).

Genotyping

C57Bl/6 and SJL mouse strains were crossed, and genotyping was performed using polymerase chain reaction (PCR) on genomic DNA extracted from ear biopsies. The designed oligonucleotide primers are listed in Supplementary File 1. The PCR cycling conditions were as follows: 3 min at 94 °C, followed by 35 cycles of 30 s at 94 °C, 60 s at 57.3 °C, and 60 s at 72 °C, with a final extension of 2 min at 72 °C. PCR products were resolved on a 1.5% agarose gel using Tris–acetate-EDTA running buffer and 1X Gel Loading Dye (NEB B7021-S), and bands were observed after a 45-min run at 100 V (Supplementary File 1).

Animal Housing Conditions

Mice were housed in individually ventilated cages with a 12:12 light/dark cycle at a constant temperature of 22 ± 2 °C. They had ad libitum access to food and water. To reduce environmental impoverishment, the mice were group-housed (4–5 mice per cage).

Breeding and Experimental Groups

The animals used in this study were generated by breeding 5xFAD transgenic female (B6SJL-Tg) mice with hybrid male mice (e.g., C57BL/6 J x SJL or B6SJLF1). The resulting offspring were genotyped and classified as either transgenic (Tg +) or non-transgenic (Tg-). The experimental group (TG) consisted of 5xFAD transgenic newborn mice (Tg +), while the control group (CTR) comprised age-matched non-transgenic (Tg-) mice of both sexes. A total of 46 animals from all groups and both sexes were used in this study.

Disease Progression and Euthanasia

These mice exhibit Aβ plaque deposition and gliosis at 2 months of age, synapse loss and cognitive impairment after 3 months, and loss of layer 5 cortical neurons by 6 months of age [36]. All mice were euthanized at 3, 6, and 9 months of age for analysis.

Detection of Amyloid *Beta* Deposit by Congo Red Staining

Congo red staining was performed as previously described [37] with slight modifications. Brain sections were washed three times in phosphate-buffered saline (PBS). The sections were mounted onto slides. Before staining, the tissues were first fixed in PBS for 15 min and then in methanol until dry (15 min) at room temperature. Tissue sections were then incubated in NaCl solution for 5 min, followed by a 30-min incubation in Congo Red dye (Sigma-Aldrich, Taufkirchen, Germany). Stained sections were rinsed eight times each in 95% ethanol, 100% ethanol, and 100% ethanol, followed by two times 5-min incubation in xylene and mounting with Entellan (Supplementary File 2).

Western Blotting

A total of 24 numbers of 3-, 6-, and 9-month-old male and female mice ($n = 4$ CTR, $n = 4$ TG) were used for Western blot analysis. All procedures related to animal husbandry and euthanasia were approved by the Acibadem Mehmet Ali Aydinlar University Animal Experiments Local Ethics Committee. Mice were anesthetized with isoflurane (1–2% oxygen) for the duration of the procedures. Following anesthesia, the hippocampal tissues were dissected and immediately frozen in liquid nitrogen. These tissues were stored at − 80 °C until protein extraction.

The hippocampal tissues were homogenized in ice-cold RIPA lysis buffer (50 mM Tris–HCl, pH 7.4, 150 mM NaCl, 1% NP-40, 0.25% sodium deoxycholate, 1 mM Ethylenediaminetetraacetic Acid (EDTA), 1 mM phenylmethylsulfonyl fluoride (PMSF), 1 mM sodium orthovanadate, 1X protease inhibitor cocktail with 1 mM sodium fluoride) using a tissue Dounce homogenizer. Homogenized samples were then sonicated with an Omni Ruptor 4.000 sonicator for approximately 1 s. PBMC cell lysates were prepared in RIPA lysis buffer. Lysates were centrifuged at 14,000 × *g* for 15 min at 4 °C to collect supernatants. The extracted protein concentration was measured using the Bradford protein assay (Bio-Rad, USA).

Twenty micrograms of protein from each sample was separated by 10% and 12% SDS–polyacrylamide gel electrophoresis, then transferred to a nitrocellulose or PVDF membrane using a semi-dry transfer system (40 min, 25 V) (Bio-Rad, Transblot). Membranes were incubated with 5% bovine serum albumin for 1 h at RT. The membranes were then incubated with primary antibodies against DRP1 (1:1000, Santa Cruz Biotechnology, USA), MFN2 (1:1,000, Cell Signaling Technology, USA), OPA1 (1:1,000, BD Transduction Laboratories, USA), phospho-DRP1 (pDRP1) S616 (1:1000, ABclonal, USA), and β-actin (1,10,000, Thermo Fisher Scientific, USA) overnight at 4 °C. The membrane was rinsed three times with TBS-T for 10 min and then probed with appropriate secondary antibodies 1:2000 (rabbit for pDRP1 (S616), MFN2, VDAC and PINK1: and mouse for DRP1 and OPA1, TOM20) and 1:10,000 (mouse for actin) for 1 h at RT, followed by three washes with TBS-T for 10 min. Protein bands were visualized with an enhanced chemiluminescence reagent (SuperSignal™ West Femto Maximum Sensitivity Substrate, Thermo Scientific, USA). Finally, the relative intensities of the protein bands were analyzed with Image Lab software (Bio-Rad, USA) and the

ImageJ (RRID: SCR_003070) computer program (NIH, USA).

Electron Microscopy

Tissue Fixation For electron microscopy, a total of 6 mice (3 CTR, 3 TG) were used. The sex of the animals was not noted. All animal procedures were approved by the Acibadem Mehmet Ali Aydinlar University Animal Experiments Local Ethics Committee. Mice were deeply anesthetized with an excess dose of ketamine (100 mg/kg) and xylazine (20 mg/kg) IP, and then, they were perfused transcardially with 100 ml of Tyrode's solution (137 mM NaCl, 2 mM KCl, 0.9 mM CaCl2, 1.2 mM MgCl2, 11.9 mM NaHCO3, 0.4 mM NaH2PO4, 5.5 mM glucose, pH 7.4, osmotic strength 281 mOsm), followed by 4% paraformaldehyde and 0.5–1% glutaraldehyde in 0.1 M phosphate buffer (PB; pH 7.4) as fixatives. All perfusates were kept at room temperature. The brains were then removed and post-fixed in 4% paraformaldehyde in 0.1 M PB (pH 7.4) overnight. The following day, each brain was dissected sagittally, with each hemisphere block placed in a vibratome and sectioned at 60 µm. The sections were immediately treated with 1% sodium borohydride, and the free-floating sections were kept at 4 °C in 0.01 M PBS containing 0.1% sodium azide.

Tissue Processing for Electron Microscopy The sections were processed for electron microscopy (EM) at Acibadem University, following previously described protocols [38]. Briefly, the sections were treated with 1% osmium tetroxide in 0.1 M PB for 1 h. The sections were then rinsed in 0.1 M PB three times for 3 min each and dehydrated using 50% ethanol (ETOH) for 3 min, 4% filtered uranyl acetate in 70% ETOH for overnight at 4C, 70% ETOH for 1 mi, then 90% ETOH for 5 min, and 100% ETOH twice for 5 min each at room temperature. The sections were further dehydrated in acetone three times for 2 min each, followed by resin infusion in a 1:1 mixture of acetone and Epon overnight. Then, the sections were placed in pure Epon overnight. The sections were then flat embedded between two Aclar sheets (EMS) and placed in a 60 °C oven overnight for polymerization. After marking the area of interest (CA1 region) on the selected tissue section with the help of a light microscope, sections were excised from the flat embed, placed on the cap of the BEEM capsules, filled with Epon, and polymerized in a 60 °C oven overnight. Using a camera lucida outlines and landmarks of sections were drawn to further identify and specify the 1 × 2 mm area of interest, which was then cut into 60-nm sections using a Leica Ultramicrotome UTC7 and collected on 400-mesh copper grids.

EM Imaging and Morphometry The ultrathin sections of the hippocampus were viewed using a JEOL1010 electron microscope equipped with a 16-megapixel CCD camera (SIA). Images of the hippocampus neuropil were captured from three regions: (1) CA1 pyramidal cell bodies; (2) the proximal dendrites of CA1 pyramidal neurons; and (3) the distal dendrites of CA1 pyramidal neurons. The latter two regions corresponded to stratum radiatum and stratum lacunosum, respectively. All images were captured at a magnification of × 10,000, yielding images at 4096 × 4096 pixel resolution.

For morphometric analysis of mitochondria, the outlines of the dendrites and the mitochondria were traced using measurement tools of FIJI ImageJ (version 1.54j), and areas and diameters were computed using Area and MinFeret tools of the ImageJ Core and Microscope Measurement Tools plugins. For MERCs distance analysis, at least 10 straight lines were drawn between the mitochondria membrane and the nearby ER, connecting the closest points; distances are captured using the length measurement tool in Image J. Distances larger than 80 nm were excluded.

Visualization of the Results Adobe Creative Cloud Photoshop was used for constructing graphs and Figs. EM images were adjusted for tiling or contrast as needed without changing content.

Flow Cytometry

A total of 16 mice ($n = 8$ CTR, $n = 8$ TG) were used for flow cytometry experiments. Blood samples of the 6- and 9-month-old mice were used by cardiac puncture [39] under low-level anesthesia (1–2% oxygen) to ensure humane handling of conscious animals. After blood collection, the same animals were then used for brain tissue extraction for Western blot analysis. PBMCs were isolated from the collected blood samples via density-gradient centrifugation using Ficoll medium [40]. The harvested PBMCs were centrifuged at 500 × *g* for 5 min and washed with 1 × PBS. Cells were immediately used for flow cytometric measurement, and trypan blue staining was performed for live and dead cell counts. From each group, 2×10^5 cells were stained with 100 nM MitoTracker Red CMXRos, 5 µM MitoSOX Red, and 50 nM MitoTracker Green FM for 20 min at 37 °C to determine mitochondrial membrane potential (MMP), mitochondrial superoxide formation (MitoSOX), and mitochondrial mass (MM), respectively. After 20 min, the samples were washed with 1 × PBS, and pellets were dissolved in 400-µL PBS and transferred to flow tubes for flow cytometry (BD FACSVerse). In this study, 10,000 events were acquired, properly gated, and analyzed using BD FACSuite. MMP and MitoSOX levels were measured in the presence of electron transport chain (ETC) complex inhibitors, rotenone, antimycin, and carbonyl cyanide 4-(trifluoromethoxy) phenylhydrazone (FCCP). For this purpose, samples were incubated with 2.5

ug/ml rotenone, 2.5 ug/ml antimycin, and 10 uM FCCP as an uncoupler for 20 min at 37 °C, washed with PBS, and then stained with fluorescent dyes as mentioned above [41–43]. A total of 10,000 events were obtained, properly gated, and analyzed using FlowJo software.

Statistical Analysis

Statistical analysis was performed using GraphPad Prism version 10.2.0 software. The data acquired from Western blotting were statistically analyzed by Mann–Whitney *U* or unpaired *t*-test to compare the ratio between the two groups. Ordinary one-way ANOVA test or Kruskal–Wallis test was used for more than one group comparison related to parametric or non-parametric data. Data are presented as mean ± S.E.M. $*p < 0.05$ was considered significant.

Datasets obtained from EM images (area, caliber, MERCs distance, mitochondria string count) are statistically analyzed using GraphPad Prism version 10.2.3 software. Non-parametric datasets (i.e., area, caliber) are analyzed by the Mann–Whitney *U* test, using $p < 0.01$ as significant. Datasets with repeated measurements (i.e., MERCs distance ratio in proximal/distal dendrites, mitochondria string count ratio) are analyzed by an unpaired *t*-test with Welch's correction, which does not assume that two populations have the same standard deviation and $p < 0.05$ as a significance factor. To test for clustering of MERC distance groups, the R package (R Project for Statistical Computing; RRID: SCR_001905) Mclust is used to perform a clustering analysis based on the best-fitting Bayesian Information Criteria (BIC) among models with varied clusters.

Results

Evaluation of Mitochondrial Dynamic-Related Protein Levels in 5xFAD Mice

Several studies pointed out that an altered expression pattern of mitochondrial fission and fusion proteins exists in AD brains, including APP and Tau mouse models, leading to a disrupted balance that contributes to mitochondrial dysfunction and neurodegeneration [30, 44–46]. To understand how proteins related to mitochondrial dynamics, including MFN2, OPA1, DRP1, and phospho-DRP1 (S616), change during the lifespan of the 5xFAD model, we examined these protein expression levels in hippocampal tissues of 3-, 6-, and 9-month-old control and transgenic animals by Western blot.

We evaluated mitochondrial fusion by measuring the MFN2 level and OPA1. MFN2 protein levels in the hippocampus of 6- and 9-month-old TG 5xFAD mice were significantly decreased compared to CTR mice ($p = 0.0078$, 0.0431, respectively) (Fig. 1D). The fold change in MFN2 levels at 3-, 6- and 9-month-old was significantly diminished in TG mice compared to CTR mice ($p = 0.0470$, 0.0098, and 0.0466, respectively) (Fig. 1D). OPA1 is required for the maintenance of mitochondrial inner membrane integrity and cristae structure. The unprocessed, N-terminal transmembrane-bound, long-form, and the non-transmembrane-bound, proteolytically processed short form are termed L-OPA1 and S-OPA1, respectively [47]. These two forms of OPA1 protein levels in the hippocampus of 6- and 9-month-old TG 5xFAD mice were significantly lower than in CTR mice (L-OPA1: $p = 0.0002$, 0.0359; S-OPA1: $p = 0.0002$, 0.0448, respectively) (Fig. 1E, F). In addition, when we normalize the CTR group's values to TG values (the fold change), L-OPA1 and S-OPA1 levels were significantly lower in TG mice compared to 6- and 9-month-old CTR mice (L-OPA1: $p = 0.0001$, 0.0001; S-OPA1: $p = 0.0001$, 0.0003, respectively) (Fig. 1E, F). This finding emphasizes that a lower OPA1 and MFN2 expression level may cause impairment in the cristae structure and mitochondrial fusion in 5xFAD mice after 6 months.

DRP1, a GTPase, is known as a critical player in the fission process. When we measured DRP1 protein levels in the hippocampus of 6-month-old TG 5xFAD mice, we observed that DRP1 levels were significantly lower than CTR mice ($p = 0.0001$) (Fig. 2C). However, in the 9-month-old animal, DRP1 levels were similar between CTR and TG at 5xFAD mice (Fig. 2D). In addition, in the 6-month-old, the fold change in DRP1 levels was significantly declined in TG mice compared to CTR and 9-month-old TG mice ($p = 0.0143$, 0.0117, respectively) (Fig. 2E). Furthermore, serine phosphorylation (S616) plays a critical role in DRP1's GTPase activity [48, 49]. To understand how pDRP1 (S616) levels also change during the development of mice, we also evaluated this protein level. In 6 months, the ratio of pDRP1 (S616) to total DRP1 significantly decreased compared to CTR mice ($p = 0.0129$ (Fig. 2C). However, at 9 months, pDRP1 (S616) levels were increased in TG mice compared to CTR mice ($p = 0.0346$) (Fig. 2D). The fold change in pDRP1 (S616) levels at 9 months was substantially elevated in TG mice compared to CTR and 6-month TG mice ($p = 0.0017$, 0.0001, respectively) (Fig. 2E). In sum, our results indicate that the change in mitochondrial dynamics begins before the progression of the disease.

Ultrastructural Alterations of Mitochondria Structure

To reveal if alterations in mitochondria-associated proteins in 5xFAD brains reflect on structure, we examined a total of 968 (575 CTR and 393 TG) mitochondria from CA1 striata radiata and lacunosum of 3 CTR and 3 PM9 TG mice

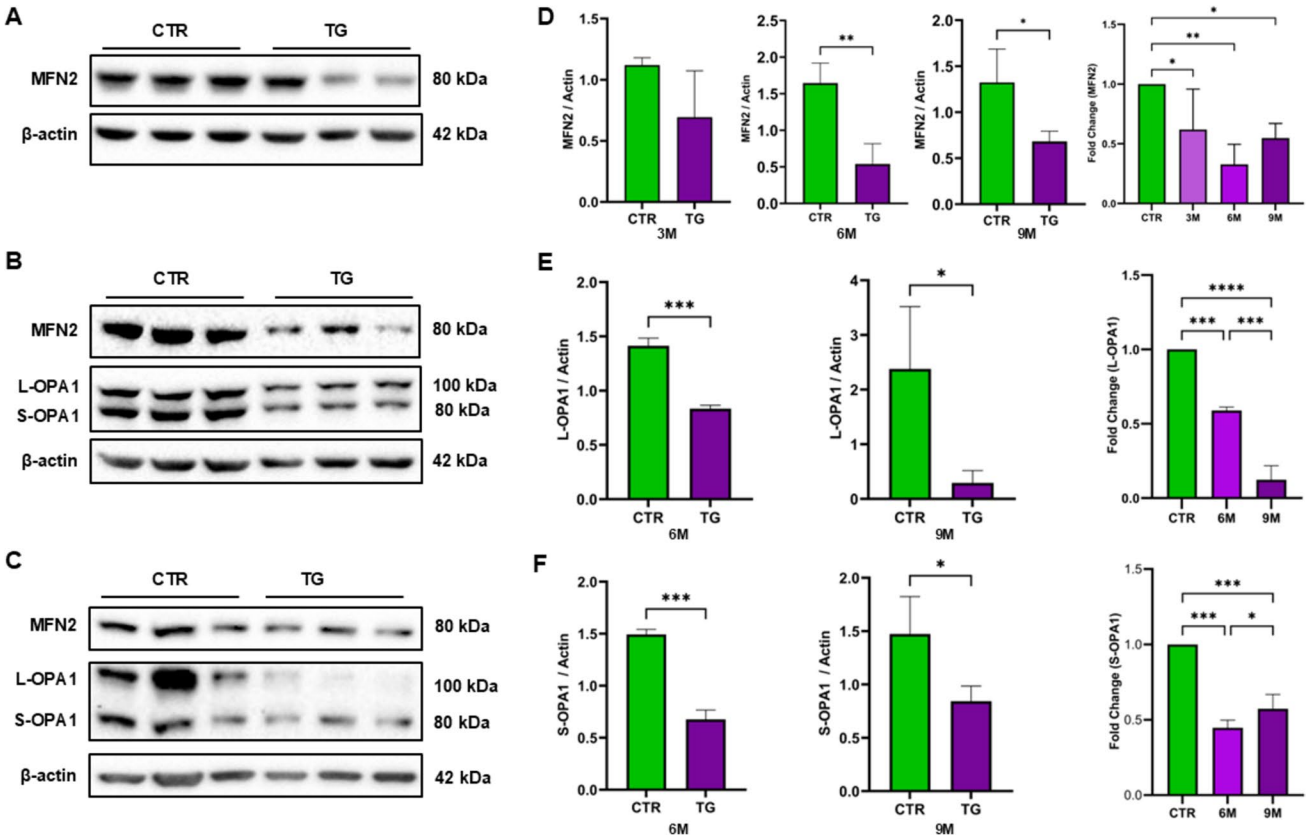

Fig. 1 MFN2 and OPA1 expression levels in hippocampal tissues of 5xFAD mice. Western blotting of MFN2 proteins in hippocampal tissues of 5xFAD mice. **A**, **D** Three-month-old; **B**, **D** 6-month-old; and **C**, **D** 9-month-old CTR and TG. OPA1 proteins in hippocampal tissues of 5xFAD mice. **B**, **E**, **F** Six-month-old and **C**, **E**, **F** 9-month-old CTR and TG. **D**, **E**, **F**) Fold change of MFN2, L-OPA1, and S-OPA1 protein level, respectively. TG group values were divided by the CTR mean, and normalization was defined as "fold change." Actin was used for internal loading control. The data represent the mean ± S.E.M. of 3 different animals in three independent experiments. For all comparisons, differences between datasets were assessed by unpaired *t*-test and one-way ANOVA with $*p<0.05$, $**p<0.005$, and $***p<0.0005$

using EM. In CTR brains, mitochondria appeared as round or elongated cross-sections, displaying tightly organized cristae, while in the 5xFAD brains, they seemed rounder and had wider cristae. The morphometric analysis of mitochondria in 5xFAD mice revealed significant alterations in mitochondrial size and distribution: mitochondria in 5xFAD mice exhibited larger areas (0.15 ± 0.1 μm^2 vs. 0.27 ± 0.2 μm^2; mean ± SD; $p<0.001$, MW-U) and diameters (0.29 μm ± 0.1 vs. 0.39 ± 0.1 μm, mean ± SD; $p<0.001$, MW-U) (Fig. 3C, D), suggesting potential alterations in mitochondrial function in the hippocampus of PM9. Although, the ratio of mitochondrial density (number of mitochondria per μm^2 of dendrite area) between proximal and distal dendrites was not statistically different between CTR and TG brains (Fig. 3E; $p=0.6476$, MW-U), a significantly lower number of mitochondria per unit area of was observed in distal dendrites of TG brains at PM9 (Fig. 3F, p = 0.0099, MW-U). The observed alterations in mitochondrial frequency may suggest that the PM9 hippocampus has fewer mitochondria, potentially reflecting a reduction in total mitochondrial mass and indicating compromised mitochondrial function.

An interesting feature of mitochondrial structure encountered in TG brains was teardrop shape: a thin-diameter extension of the mitochondria gave a paisley or tear-drop appearance to the mitochondria (Fig. 4). These long, string-like extensions are also encountered as connecting two or three mitochondrial cross-sections. Such formations are described as mitochondria-on-a-string (MOAS) and are considered a product of the incomplete fissure process [50]. While teardrop mitochondria were also encountered in CTR brains, their prevalence was significantly higher in PM9 TG brains (8.9 ± 2.1% in CTR vs. 30.7 ± 5.2% in TG (mean ± SEM); $n=3$ for each condition, $p=0.04$; unpaired *t*-test with Welch's correction; Fig. 6E). In addition, there was a non-significant trend for teardrop mitochondria to be more prevalent in the distal dendrites both in the CTR and TG brains, and no teardrop mitochondria were encountered in the somata in either condition, consistent with a deficit in the retrograde transport mechanism of TG mitochondria.

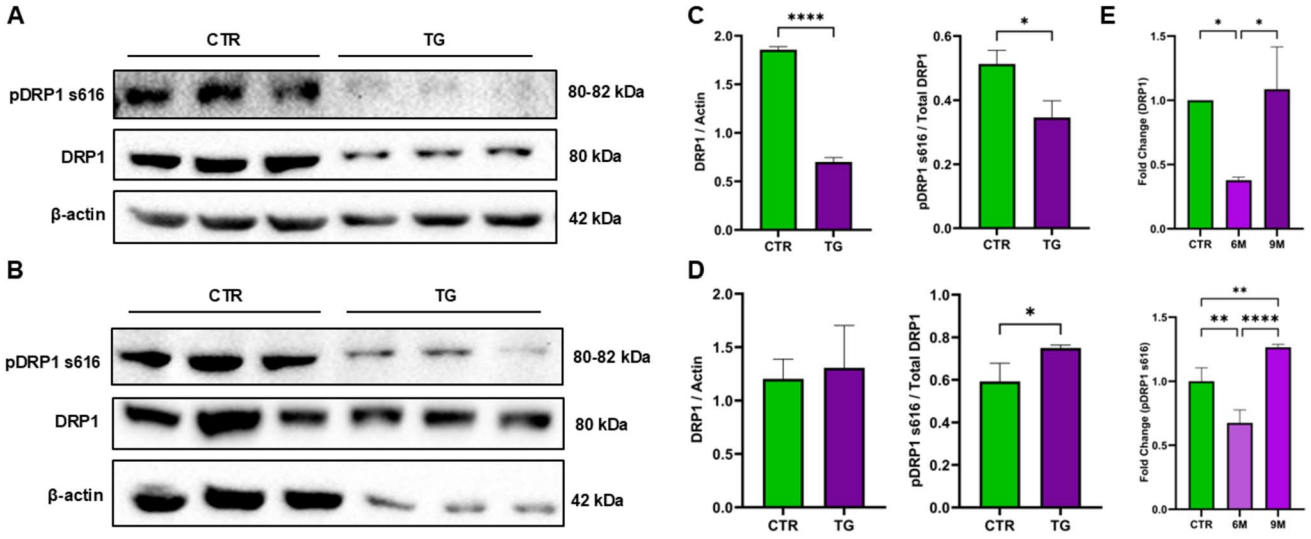

Fig. 2 pDRP1 and DRP1 expression levels in the hippocampal tissues of 5xFAD mice. Western blotting of pDRP1S616 and DRP1 proteins in hippocampal tissues of 5xFAD mice. **A**, **C** Six-month-old and **B**, **D** 9-month-old CTR and TG groups. **E** Fold change of pDrp1 S616 and DRP1 protein level. Actin was used for internal loading control. The data represent the mean ± S.E.M. of 3 different animals in three independent experiments. For all comparisons, differences between datasets were assessed by unpaired *t*-test and one-way ANOVA with $*p<0.05$, $**p<0.005$, and $***p<0.0005$

To determine the impact of amyloid overexpression in transgenic animals had an impact on the mitochondria-endoplasmic reticulum function, we measured MERCs distances in CA1 neurons from 3 CTR and 3 TG brains. A MERCs is identified as the appearance of mitochondria in close proximity to an ER, with the membranes of each structure running somewhat parallel at their cross-sections. A total of 268 MERCs (120 from CTR and 148 from TG brains encountered in CA1 pyramidal somata) were examined. Statistical analysis revealed that the distances of MERCs in TG animals were significantly greater than in CTR animals (29.5 ± 17.8 nm vs. 36.5 ± 18.9 nm (mean ± SD), $p < 0.001$, MW-U). In both CTR and TG brains, MERCs distance distributions revealed multiple subpopulations that may correspond to functional compartments (Fig. 5D, E). A BIC and clustering analysis using Mclust (Rstudio) revealed three subpopulations with cutoff points around 30 nm and 50 nm. As these cutoff points were consistent with previously published MERCs distances for four different functional compartments [21], we applied those criteria to our MERCs dataset to identify the percent distribution of four MERCs compartments in our CTR and TG datasets. This analysis revealed 0–10 nm MERCs represented 7% in CTR vs. 2% in TG, 10–30 nm MERCs represented 56% in CTR vs. 41% in TG, 30–50 nm MERCs represented 23% in CTR vs. 32% in TG, and 50–80 nm MERCs represented 14% in CTR vs. 25% in TG brains. These results may suggest that MERC with distances shorter than 30 nm may have been preferentially compromised in TG brains.

Mitochondrial Functions in PBMCs

Mitochondrial dysfunction in PBMCs has been reported in several neurodegenerative diseases, including AD and Parkinson's disease [34, 51]. Therefore, we aimed to investigate 6- and 9-month-old mice of 5xFAD for the first time. We first isolated PBMCs and then stained cells with mitochondria-specific dyes to monitor MMP (Mitotracker Red CMXRos), mitochondrial SOX (MitoSOX Red), and mitochondrial mass (MitoTracker Green FM) by flow cytometry [39]. The lymphocyte population was analyzed by gating. Although the MMP level was similar between TG and CTR animals in 6-month-old mice, MitoSOX production was increased in TG mice compared to CTR ($p = 0.0123$, 0.0180) (Fig. 6C), and mitochondrial mass was significantly lower in the TG group compared to the CTR group ($p = 0.0157$) (Fig. 6D).

On the other hand, MMP was significantly decreased in the TG group compared to the CTR group in 9-month-old mice ($p = 0.0001$, 0.0098, respectively) (Fig. 7B). In addition, MitoSOX production was increased in TG mice compared to CTR ($p = 0.0156$ and 0.0140, respectively) (Fig. 7C). Similar to 6-month-old mice, mitochondrial mass was significantly diminished in the TG group compared to the CTR group ($p = 0.0128$) (Fig. 7D).

Mitochondria have a crucial role in the production of reactive oxygen species (ROS) in the cytoplasm. During oxidative phosphorylation, there is also an electron leak and a proton leak, and this leakage plays an important role in cellular physiology and pathology [52]. Therefore, to reveal how this process is regulated in AD models, we also used ETC inhibitors and

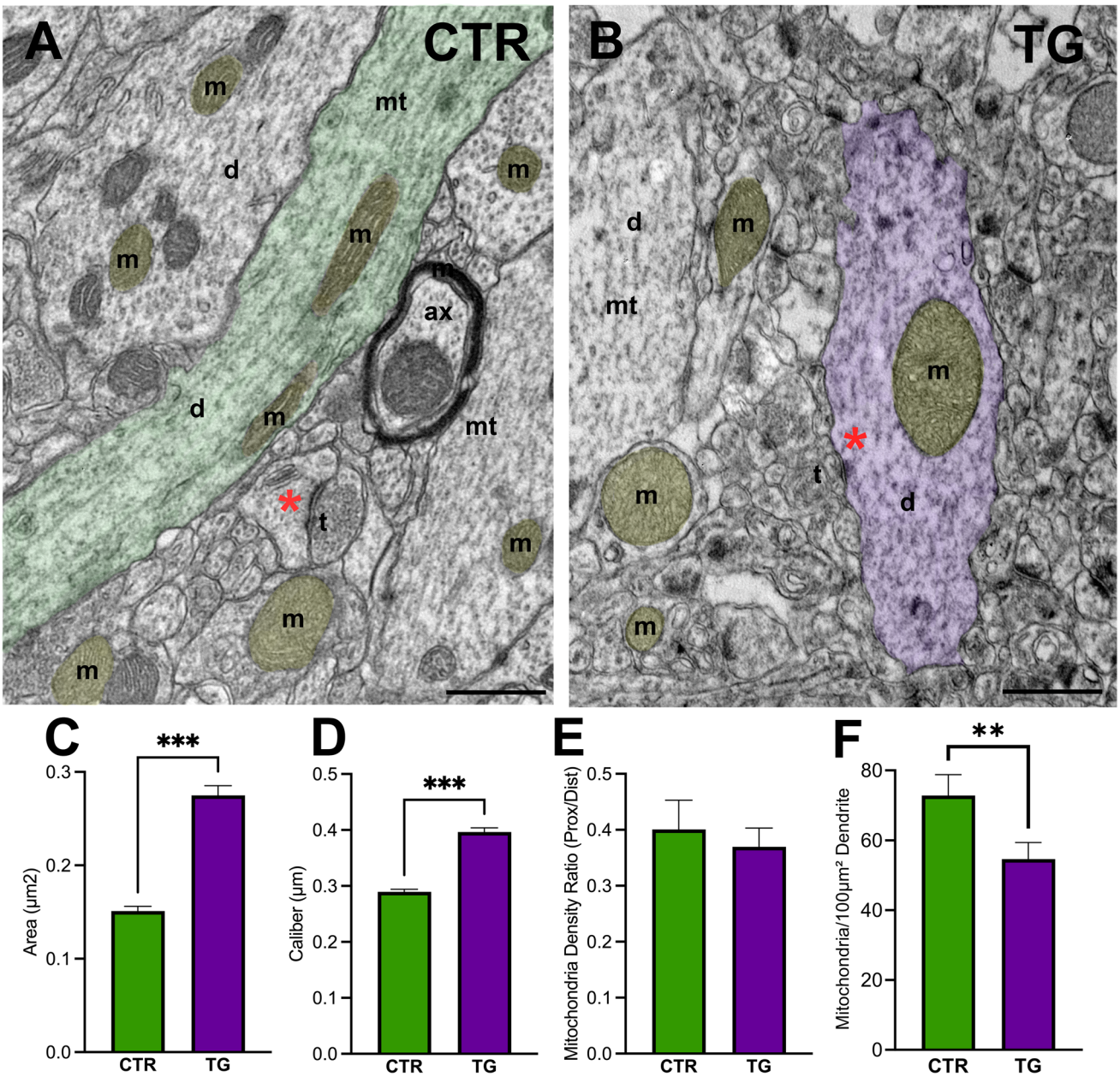

Fig. 3 Ultrastructural morphology of mitochondria. Electron micrographs of pyramidal dendrites (green in CTR, purple in TG) in the CA1 region of the hippocampus, displaying structural differences in mitochondrial (yellow) structure in CTR (**A**) and 5xFAD (**B**) mice. Scale bar: 500 nm. Abbreviations: m: mitochondria; rER: rough endoplasmic reticulum; nuc: nucleus; mt: microtubule; ax: myelinated axon; d: dendrite; t: terminal; *: synapse. **C** The mitochondrial areas in the TGmice brains are significantly larger than in CTR mice at PM9 (Mann–Whitney *U*-test $p < 0.001$). **D** Mitochondria diameter in TG animals is significantly higher in TG animals (Mann–Whitney *U*-test, $p < 0.001$). **E** The mitochondrial density ratio (number of mitochondria per µm.^{2} of dendrite area in proximal dendrites compared to distal dendrites) between CTR and TG brains ($p = 0.6476$). **F** A comparison of the number of mitochondria in the distal dendrites of control (CTR) and transgenic (TG) mice ($p = 0.0099$)

FCCP, which disrupt ATP synthesis by uncoupling the proton gradient generated by the MMP [53]. To measure impairment at Complex I and Complex III, we used rotenone and antimycin, respectively. We compared the MitoSOX level in the presence and absence of these inhibitors. As expected, in 9-month-old mice, MitoSOX levels increased upon rotenone and antimycin treatment in the lymphocyte population of control animals ($p = 0.0116$, 0,0110, respectively) (Fig. 8A, B). However, these inhibitors did not elevate MitoSOX levels in transgenic animals, indicating an impairment at the ETC level and reverse electron transport process through Complex I [54, 55]. In 9-month-old mice, when baseline MMP values were

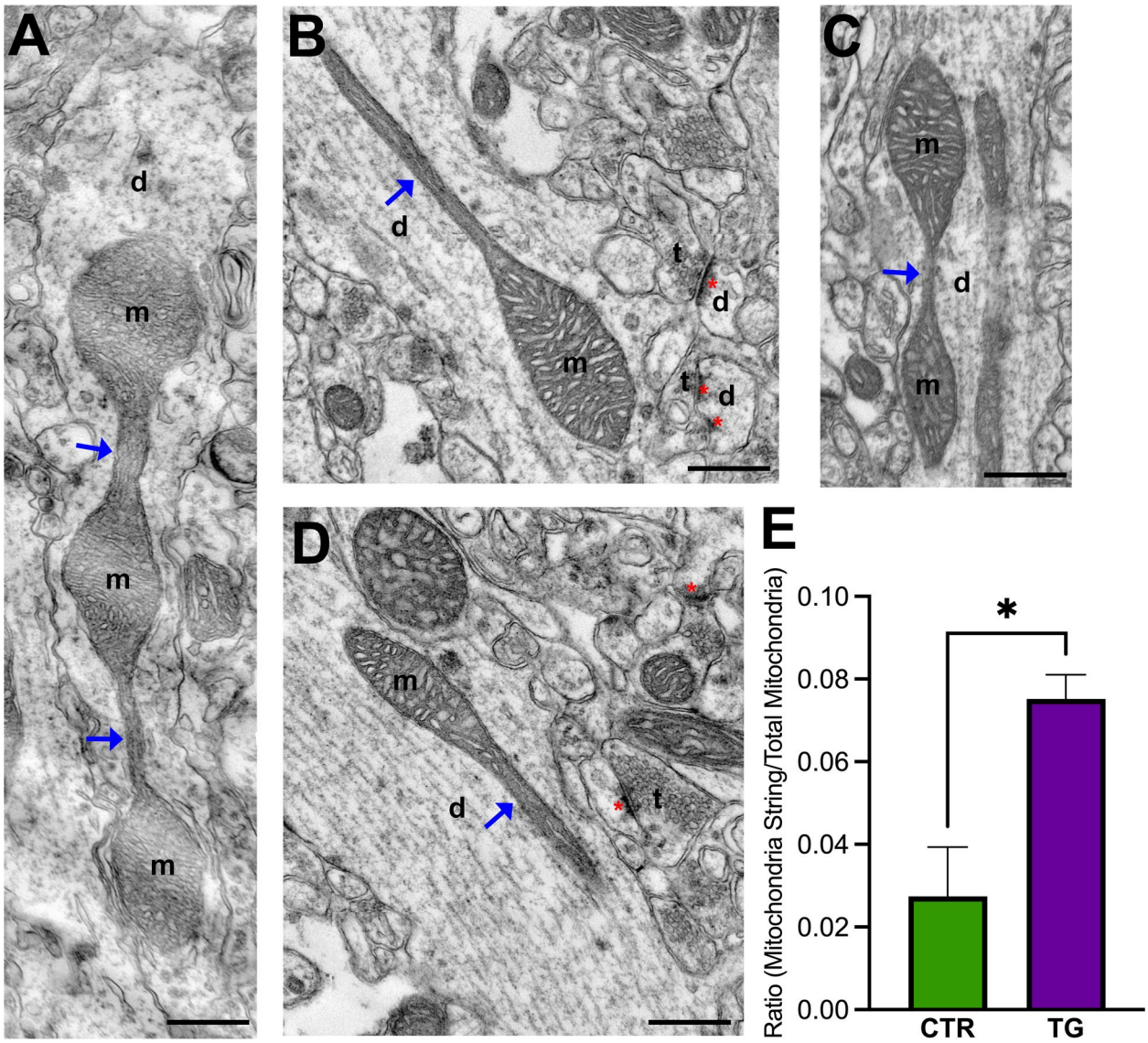

Fig. 4 Mitochondria-on-a-string structure. Mitochondria-on-a-string structures are found in TG animals. **A** Three mitochondria are connected with string-like mitochondrial extensions (blue arrows). Structures of synapses (red asterisk) and terminals can also be observed. **B–D** Teardrop-shaped mitochondria are encountered either extended as long strings or connecting other mitochondria in the cross-sections. The strings usually maintain a uniform diameter at each instance and display cristae oriented parallel to their axes. Abbreviations: m: mitochondria; d: dendrite; s: synapse; t: synaptic terminal; *: synapse. Scale bar: 500 nm. **E** The prevalence (among all mitochondria observations) of stringed mitochondria in TG animals compared to CTR animals (unpaired *t* test with Welch's correction ($n=3$, $p=0.04$)

subtracted from FCCP or rotenone-treated MMP values, there was a decrease in the CTR but not in TG animals ($p=0.0361$; $p=0.0262$, respectively), suggesting mitochondrial dysfuntion in TG mice (Fig. 8C, D)

Mitochondrial Protein Levels in Hippocampus and PMBCs

To correlate changes in mitochondrial mass in PBMCs and decrease mitochondrial number in distal dendrites of hippocampus, we measured voltage-dependent anion channel proteins (VDAC) and translocase of outer membrane (TOM)20 levels, which are ubiquitously located in the outer membrane of mitochondrial in PBMCs and hippocampus tissue of 9-month-old mice. Western blot analysis demonstrated that VDAC protein levels in the hippocampus of 9-month-old TG 5xFAD mice were similar to CTR mice (Fig. 9A, B). However, TOM20 levels were significantly lower in TG mice compared to CTR mice ($p=0.0010$) (Fig. 9A, B). When we evaluated the same protein levels in PBMCs of 9-month-old mice, VDAC protein levels in the PBMCs of 9-month-old TG 5xFAD mice were significantly

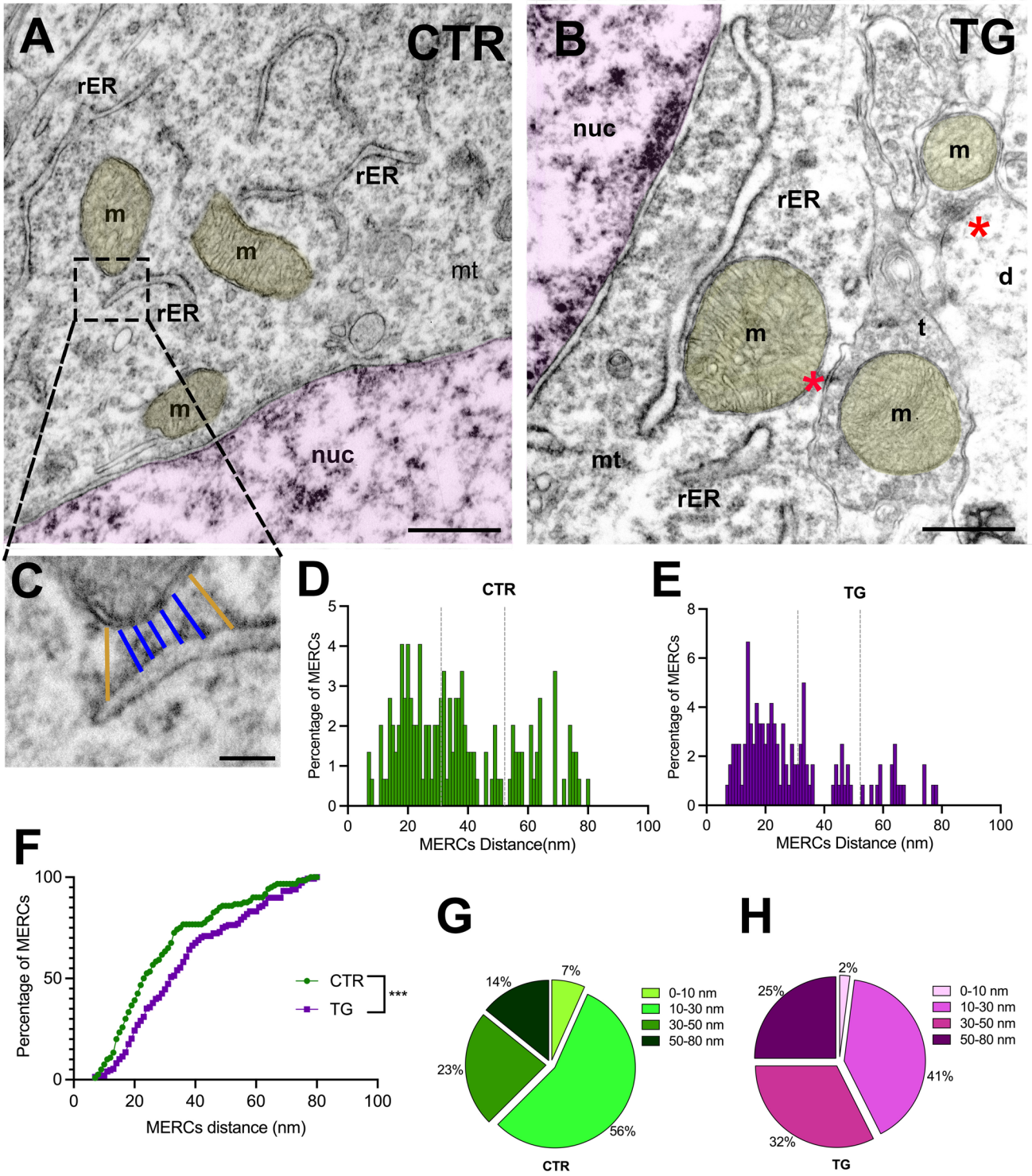

Fig. 5 Mitochondria-ER complex. Examples of Mitochondria-Endoplasmic Reticulum Contact Sites (MERCs) in CA1 pyramidal neuron somata from CTR (**A**) and 5xFAD (**B**) mice. The mitochondria (yellow) and nucleus (pink) are pseudocolored. Scale bar: 500 nm. **C** The inset illustrates the methodology for measuring MERC distances (blue lines). Distances longer than 100 nm (brown lines) were excluded from the analysis. Scale bar: 100 nm. Abbreviations: m, mitochondria; rER, rough endoplasmic reticulum; nuc, nucleus; mt, microtubule; d, dendrite; t, terminal; *, synapse. Frequency distribution histograms of MERCs in CTR (**D**) and TG (**E**) brains revealed multiple distinct subpopulations. The cutoff values (vertical dashed lines) for the subpopulations of the current dataset are obtained from the MClust BIC analysis. **F** Cumulative frequency distributions illustrate the differences between CTR and TG animals (Mann–Whitney *U*-test, $p < 0.001$). The percentage contributions of MERCs at 10 nm, 30 nm, 50 nm, and 80 nm intervals within the overall dataset in CTR (**G**) and 5xFAD TG (**H**) mice

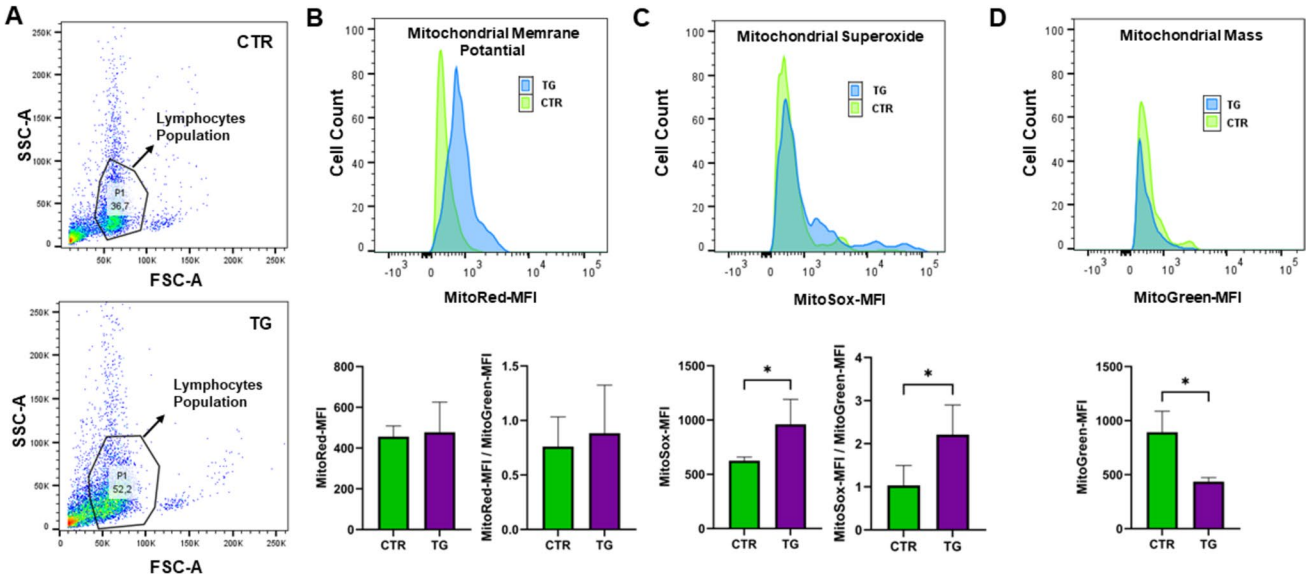

Fig. 6 Analysis of mitochondrial membrane potential, mitochondrial superoxide production, and mitochondrial mass in PBMCs of 6 months CTR and TG animals. The lymphocyte population of PBMC for CTR and TG groups (**A**) was gated according to their light scattering properties in SSC and FSC modes and 10,000 events were collected per sample. (**B**) Histogram graph showing representative of Mean Fluorescence Intensity (MFI) of MitoTracker Red CMXRos, MitoSOX, and MitoTracker Green fluorescent probes for the measurement of mitochondrial membrane potential (MMP) (**B**), mitochondrial SOX production (**C**), and mitochondrial mass (**D**), respectively. **B**–**D** Bar graphs show the MFI values of these fluorescent probes. In addition, to normalize MMP and MitoSOX, the red/green and sox/green ratios were calculated, respectively. The data represent the mean ± S.E.M. of 4 different animals. For all comparisons, differences between datasets were assessed by unpaired *t*-test with $*p < 0.05$, $**p < 0.005$, and $***p < 0.0005$. Statistical analysis was performed using GraphPad Prism version 10.2.0 software

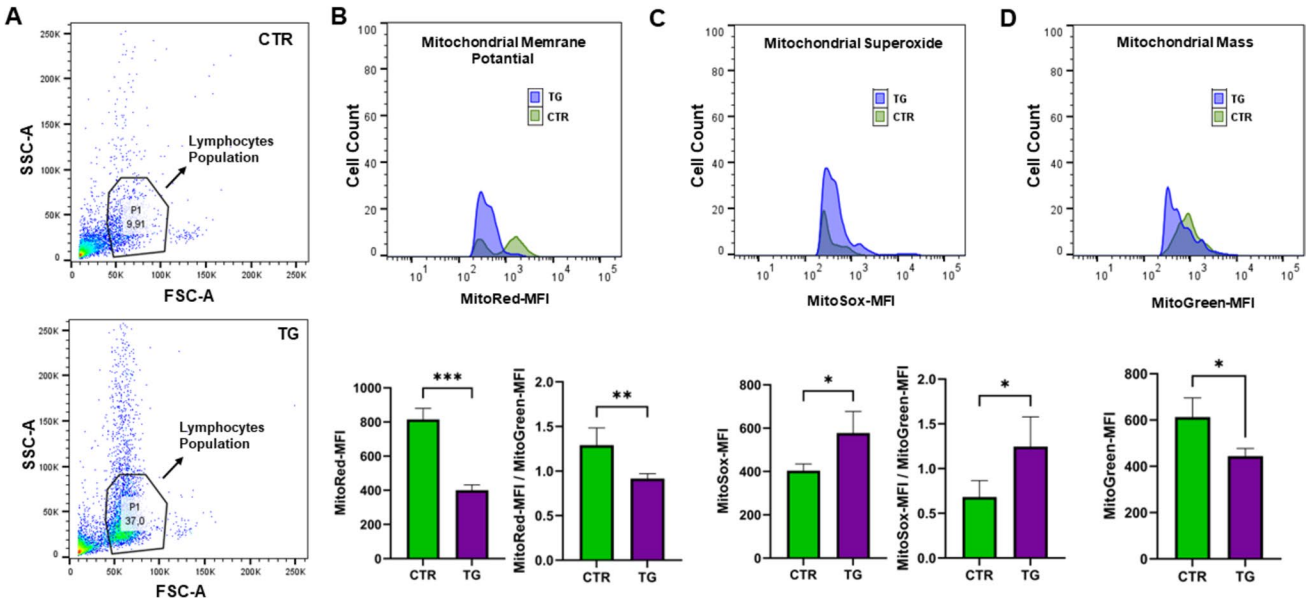

Fig. 7 Mitochondrial membrane potential, mitochondrial superoxide, and mass analysis in 9-month CTR and TG animals. Lymphocyte population of PBMC for the CTR and TG groups (**A**). Histogram plot representing the MFI of the fluorescent probe as described in Fig. 8, MMP (**B**), mitochondrial SOX production (**C**), and mitochondrial mass (**D**). Bar graphs show the MFI values of these fluorescent probes. In addition, to normalize MMP and MitoSOX, the red/green and sox/green ratios were calculated, respectively (**B**, **C**). MFI value of MitoTracker Green fluorescent probes (**D**). The data represent the mean ± S.E.M. of 4 different animals. For all comparisons, differences between datasets were assessed by unpaired *t*-test with $*p < 0.05$, $**p < 0.005$, and $***p < 0.0005$. Statistical analysis was performed using GraphPad Prism version 10.2.0 software

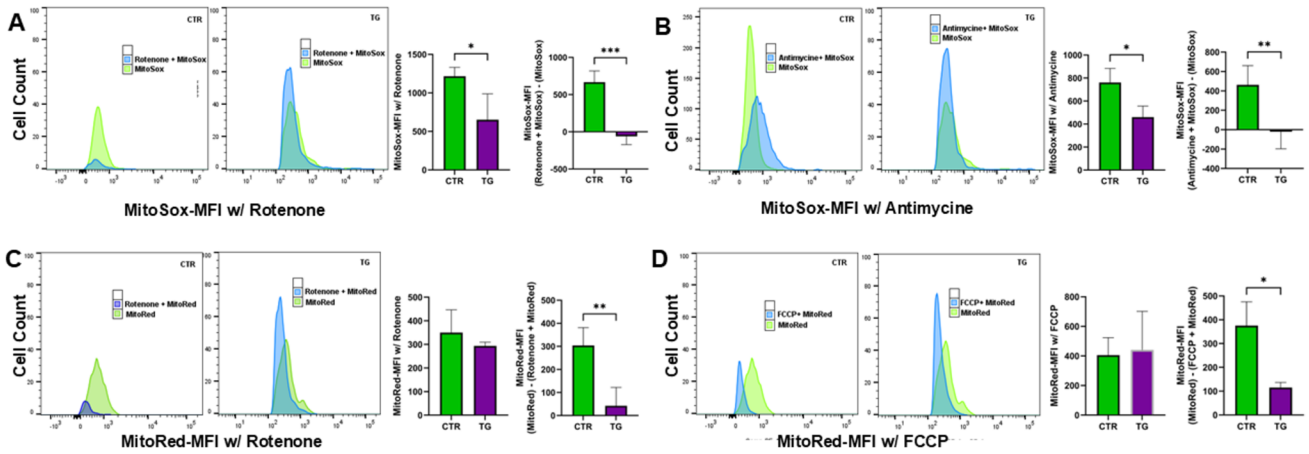

Fig. 8 Mitochondrial membrane potential, mitochondrial superoxide, and mass analysis using mitochondrial electron transport complex inhibitors in 9-month-old CTR and TG animals. Histogram plot representing the MFI of the fluorescent probe as described in the figure. Mitochondrial SOX production (**A**, **B**), MMP (**C**, **D**). Bar graphs show the MFI values of these fluorescent probes in the presence of an inhibitor and the MFI value read in the presence of an inhibitor subtracted from the value read in the absence of an inhibitor; rotenone (**A**, **C**), antimycin (**B**), and FCCP (**D**). The data represent the mean ± S.E.M. of 4 different animals. For all comparisons, differences between datasets were assessed by unpaired *t*-test with $*p < 0.05$, $**p < 0.005$, and $***p < 0.0005$. Statistical analysis was performed using GraphPad Prism version 10.2.0 software

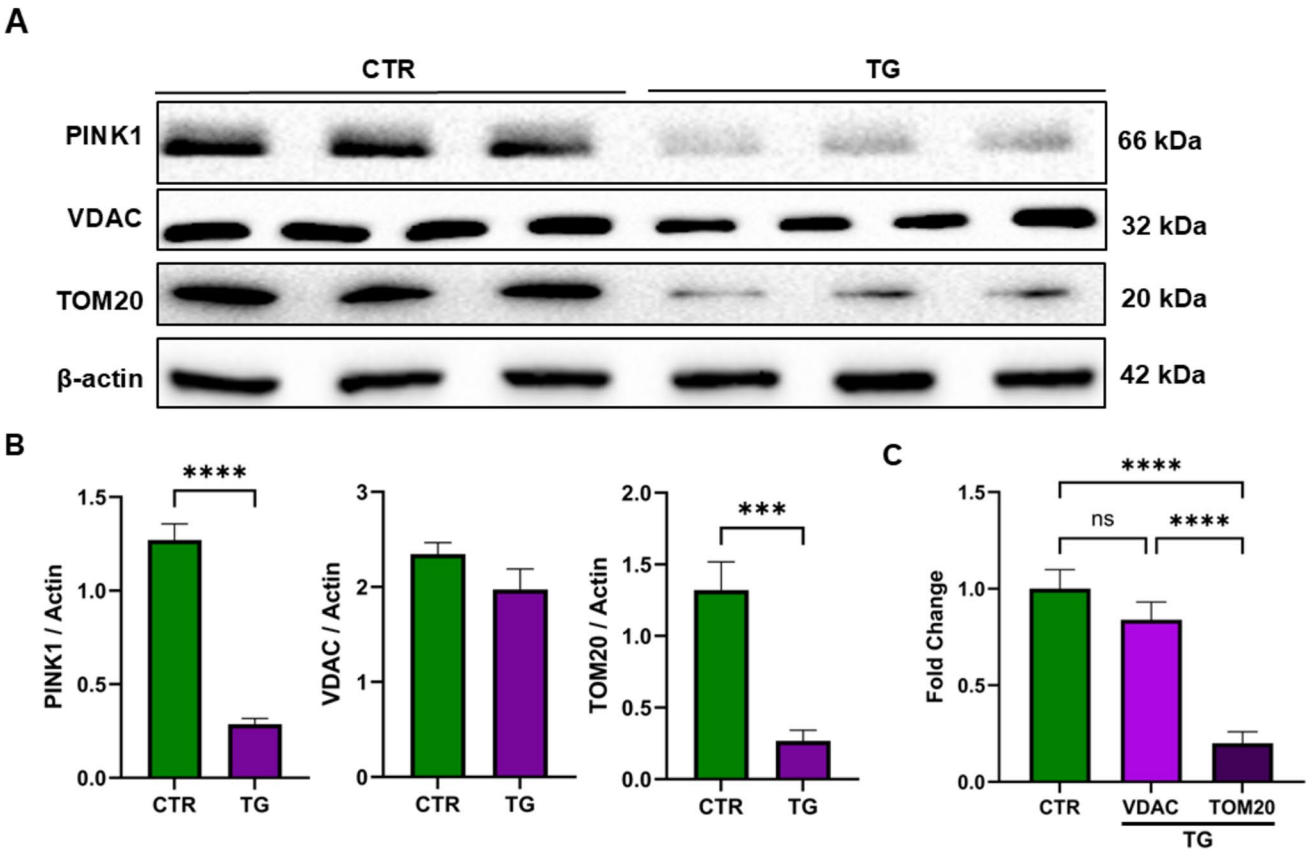

Fig. 9 PINK1, VDAC, and TOM20 expression in hippocampal tissues of 9-month-old 5XFAD mice. Western blotting of PINK1, VDAC, and TOM20 proteins in hippocampal tissues of 5XFAD mice. **A** WB figure; **B** barplot; **C** fold change. Actin was used for internal loading control. The data represent the mean ± S.E.M. of 3 different animals of three independent experiments. For all comparisons, differences between datasets were assessed by un-paired *t*-test and one-way ANOVA with $*p < 0.05$, $**p < 0.005$, $***p < 0.0005$

higher than in CTR mice ($p=0.0286$) (Fig. 10A, B). In addition, although TOM20 levels were lower in TG mice compared to 9-month-old CTR mice, this was not statitistaclly significant ($p=0.1143$) (Fig. 10A, B).

Moreover, we also assessed the PTEN-induced kinase 1 (PINK1) level in these samples. PINK is known as a serine serine/threonine kinase which is involved in the mitophagy process to remove unhealthy mitochondria [21, 56]. Similar to TOM20 levels, PINK1 levels decreased in both samples of TG mice ($p=0.0001, 0.0257$) (Figs. 9 and 10A, B). Furthermore, MFN2 level was also examined in the PBMC samples. Similar to hippocampus tissue, MFN2 declined in TG mice compared to CTR ($p=0.0295$) (Fig. 10A, B).

Discussion

Mitochondrial dysfunction and altered bioenergetics are indicators of AD. However, it remains unclear whether these changes are causes or consequences of proteinopathies in AD [57, 58]. While microglia and astrocytes in the central nervous system (CNS) were previously considered the primary contributors to AD pathologies, recent studies have underscored the involvement of peripheral immunity in both direct and indirect ways in the progression and pathogenesis of AD. Other studies have also demonstrated that chemokines or cytokines in the systemic milieu shown to impair adult neurogenesis and cognitive function in an age dependent manner in mice [56, 59–62]. According to the "mitochondrial cascade hypothesis," early changes in AD progression are mitochondrial dysfunction. In addition, this hypothesis proposes that alteration in mitochondrial function is not only implicated in the brain but also the periphery [56, 63, 64]. It is crucial to understand the crosstalk between the brain and the peripheral systems to maintain energy homeostasis [34].

Unlike previous studies focusing on changes in mitochondrial dynamics in AD, our research examined the levels of proteins associated with mitochondrial dynamics at different ages (3, 6, and 9 months old) in the brain and peripery of 5xFAD transgenic mice as a familiar type of AD. In particular, our findings demonstrated that mitochondrial fusion-related

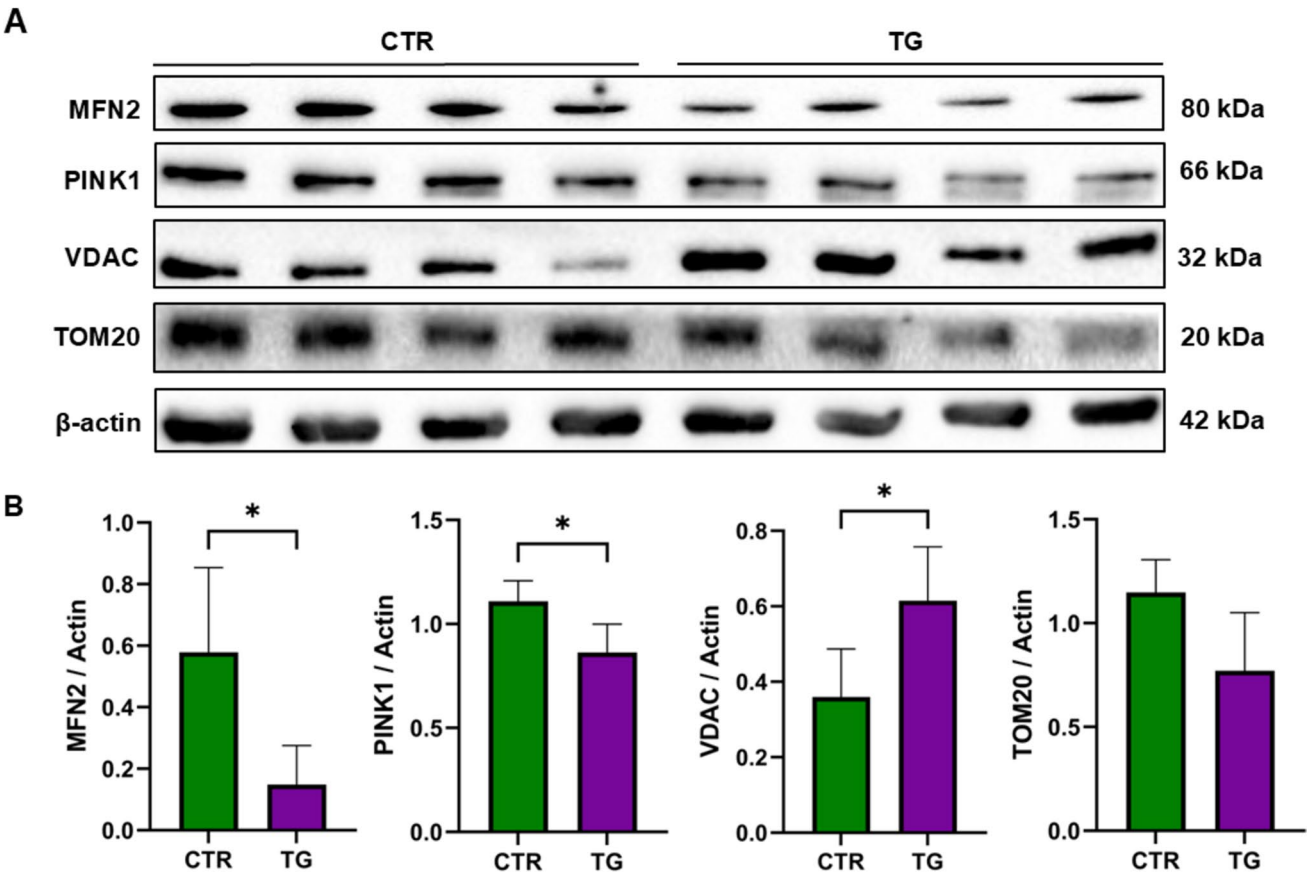

Fig. 10 MFN2, PINK1, VDAC, and TOM20 expression in PBMCs of 9-month-old 5XFAD mice. Western blotting of PINK1, VDAC, and TOM20 proteins in PBMCs of 5XFAD mice. **A** WB figure; **B** barplot. Actin was used for internal loading control. The data represent the mean ± S.E.M. of 4 different animals of three independent experiments. For all comparisons, differences between datasets were assessed by unpaired *t*-test with $*p<0.05$, $**p<0.005$, and $***p<0.0005$

protein OPA1 and MFN2 levels in the TG group were significantly lower than the CTR group in 6- and 9-month-old mice. However, the mitochondrial fission protein, DRP1, and pDRP1 were higher in 9-month-old compared to 6-month-old mice of TG animals. Wang et al. showed that DRP1, OPA1, and MFN2 levels were significantly lower in post-mortem brains of AD patients [65]. We also found low levels of OPA-1 and MFN2 in the late stages of AD. Recent studies highlighted that DRP1 interactions with Aβ and hyperphosphorylated Tau in AD cause mitochondrial dysfunction [65, 66]. DRP1 is a member of the dynamin GTPase family, and post-translational modification, including phosphorylation, is known as a critical step for its activity. Phosphorylation of the serine 616 residues of DRP1 promotes mitochondrial fission. We also investigated the pDRP1 (S616) level in this 5xFAD animal model. The level of pDRP1 at S616 enhanced in 9 months, which was consistent with neuronal cell lines [67]. Furthermore, a few studies demonstrated that inhibition of DRP1 activity rescues mitochondrial fragmentation in cell lines and animal models of AD, suggesting a regulatory role of DRP1 activity in AD [68, 69].

Furthermore, impaired mitochondrial fission due to dysregulation of the fission machinery may lead to changes in mitochondrial shape [70]. To visualize the mitochondrial morphology of hippocampal tissues from 5xFAD animals, we performed TEM analysis. Our data pointed to major alterations to mitochondrial structure and function in 5xFAD brains, including abnormalities in mitochondrial size and shape and the predominance of teardrop mitochondria. Moreover, changes in MERCs distances may have an influence on mitochondria-ER function in transgenic brains. MERCs with a 10-nm cleft distance could be used for lipid transfer, and MERCs with a 10 to 30-nm cleft width are thought to be used for calcium transfer [24]. Our results revealed the difference between CTR and TG groups for the MERCs distance, especially for 10–30 nm and 30–50 nm. A few studies indicated that presenilin 2 mutations can cause an increase in the ER-mitochondria binding and the Ca^{2+} flux at the cellular level [71, 72]. Given 30–50 nm is responsible for the Ca^{2+} flux, our data provide further insight at the organism level. Moreover, OPA1 and MFN2 are also involved in cristae structure and ER-mitochondrial juxtaposition, respectively, together with the ultrastructural changes and reduction of OPA1 and MFN2 levels found in our study give an additional clue for the modulation of mitochondrial dynamics.

Given neurons demand metabolic adaptations, mitochondrial transport within neurons plays a crucial role in maintaining neuronal health. There are two main axonal transport directions: one is called axonal transport from the cell body to the axon terminal (anterograde transport) and, in contrast, back toward the cell body (retrograde transport). Mitochondrial transport to synapses is dependent on microtubules in both axons and dendrites. However, mixed polarity is seen in the proximal dendrites. There are a few studies illustrating the impairment of mitochondrial transport in AD [2, 73]. In our study, we measured the number of mitochondria in proximal and distal dendrites. This suggests that the accumulation of the teardrop-shaped mitochondria in the distal dendrites may be an outcome of a disrupted retrograde transport mechanism.

Although the control group animals had a higher number of mitochondria at distal dendrites, the ratio in the proximal and distal regions was similar. On the other hand, our analysis of the localization and the prevalence of teardrop shape revealed that such morphologically distorted mitochondria were more plentiful in the distal dendrites of aged control animals, and their ratio in the distal dendrites was substantially increased in transgenic animals. Previous studies indicated that mitochondrial fission arrest results in elongated linked organelles, a phenotype called "mitochondria-on-a-string" (MOAS). The MOAS phenotype likely reflects deficits in the selective elimination of damaged mitochondria, aggravating metabolic deficits, and ROS production [50]. To date, only a few studies have documented MOAS morphology in different AD models or post-mortem human brains [69, 70, 74]. Our data confirms these morphological changes in 5xFAD mice as well. However, the changes in MERCs distance remain elusive in animal models or post-mortem human brains. Our results revealed the difference between CTR and TG groups for the MERCs distance, especially for 10–30 nm and 30–50 nm. Since MERCs are involved in different biological functions, including lipid and Ca2 + ion exchange and autophagosome formation, a decrease in distance MERCs might be related to altering these functions in AD. Moreover, it has been reported that more than 20 proteins, including VDAC1, OPA1, and MFN2, are involved in the controlling of MERCs tethering; the long distance in MERCs may be implicated in the reduction in OPA1 and MFN2 levels in 5xFAD [63, 75].

Our study emphasizes that mitochondrial dysfunction starts in the early stages of 5xFAD mice and not only in the brain tissue of animals but also in the periphery. Although abnormalities in mitochondrial dynamics and oxidative stress are associated with AD's pathogenesis, mitochondrial dysfunction in the peripheral tissues of AD patients and the AD mouse model is not well established. There are contradictory studies based on the respiratory chain complex activity, mitochondrial respiration, platelets, and lymphocytes of AD patients [76–79]. In addition to the hippocampal tissue of the 5xFAD mouse model, we also measured the mitochondrial function of peripheral blood mononuclear cells. Our results revealed that MMP and mitochondrial mass decreased and MitoSOX increased in PBMCs of the late stage of 5xFAD animals, indicating impairment in mitochondrial respiration. Apart from the others, we also evaluated reverse electron transport activity using a complex I inhibitor (Rotenone) [54]. We found an impairment of

complex I and complex III activity during the development of 5xFAD animals. Our results now provide further evidence that blood lymphocytes are an early peripheral sign for the diagnosis of AD and that they are detected in the blood of as early as 6-month-old mice in the 5xFAD model.

To correlate changes in mitochondrial mass in PBMC and hippocampus, we studied VDAC, TOM20 protein levels. Our results revealed that the VDAC level did not change in the hippocampal tissue; however, it increased in the PBMCs of TG mice. Since several studies indicate that VDAC interacts with amyloid beta and this protein accumulates on mitochondria upon amyloid treatment or in the brain of AD patients, we also checked the TOM20 protein level [80–82]. Interestingly, in contrast to VDAC, TOM20 showed a significant reduction in both samples. The reduction in TOM20 levels, as determined by Western blot analysis, correlates with alterations in mitochondrial mass in PBMCs, as assessed by flow cytometry. Moreover, the decline in MFN2 levels in hippocampal tissue can be associated with the subsequent reduction in mitochondrial mass [2, 65]. Given the observed reduction in mitochondrial number in TG, the unaltered VDAC levels may be attributed to an increase in its expression, as observed in other studies. In addition, the low level of PINK1 can be associated with defective mitophagy, which was previously reported in several studies [21, 56].

Some limitations of our study should be described. Incorporating 12-month-old mice would yield more detailed data regarding mitochondrial dynamics in AD. Due to difficulties in breeding transgenic mice, we could not separate gender differences. We were unable to take into account the impact of sex differences due to difficulties in breeding transgenic mice. In addition, our control animals were transgenic littermates (BLSJL-Tg strain), not wild-type. Although our results revealed an alteration of mitochondrial dynamics between non-transgenic and transgenic animals, comparing transgenic mice with wild-type mice would have increased the consistency of our results and minimized genetic variability. Moreover, the small size of the mice hindered our ability to perform certain experiments and repeat tests, further limiting the scope of our analyses. Despite these challenges, we believe our findings still offer valuable insights into mitochondrial alterations associated with AD.

In conclusion, our findings highlighted for the first time comprehensive mitochondrial changes in both central and peripheral tissues of 5xFAD and proposed that peripheral markers of mitochondrial dysfunction may serve as significant biomarkers for AD. Given that understanding the intricate relationship between mitochondria and AD pathology is crucial, our results may contribute to targeting new therapeutic strategies, including modulating OPA1, MFN2, and DRP1 activity or electron transport complex activity, that may help alleviate the impact of this devastating neurodegenerative disorder.

Supplementary Information The online version contains supplementary material available at https://doi.org/10.1007/s12035-024-04632-4.

Acknowledgements The authors are grateful to Acibadem Mehmet Ali Aydinlar University Faculty of Medicine, Department of Histology and Embryology, Associate Professor Dr. Merve Acikel Elmas, Institute of Health Sciences Medical Biotechnology PhD Student Gokcen Ozgun, and Ms. Rebecca Roberts of the University of Virginia for their technical assistance during tissue preparation, and to Acibadem Mehmet Ali Aydinlar University Institute of Health Science MSc students Simge Senay, Berkcan Koc, and technician Tugce Demir Ozupek for technical assistance during some parts of flow cytometry experiments.

Author Contribution Elif Nedret Keskinoz: designed the study, supervised the project, conducted and performed the experiments, carried out electron microscopic tracking of tissues, interpreted the results, prepared supplementary Figs. 1–2, and wrote and reviewed the main manuscript text. Musa Celik: performed and analyzed western blot and flow cytometry experiments, wrote the main manuscript text, and prepared Figs. 1, 2, 6, 7, 8, 9 and 10, and supplementary Figs. 3. Ezgi Sila Toklucu and Kerem Birisik: performed and analyzed electron microscopy experiments, wrote the main manuscript text, and prepared Figs. 3, 4 and 5. Alev Erisir: supervised the study, interpreted the results, conducted Figs. 3, 4 and 5, and wrote and reviewed the main manuscript text. Devrim Oz Arslan: designed the study, supervised the project, conducted and performed the western blot and flow cytometry experiments, interpreted the results, conducted Figs. 1, 2, 6, 7, 8, 9 and 10 and supplementary Figs. 3, and wrote and reviewed the main manuscript text.

Funding This research was supported by funds from the Scientific and Technological Research Council of Turkey (TÜBİTAK) under the 3501 Career Development Program, project number 219S307 to EK and DOA. The financial support for the study was provided by TÜBİTAK to EK and DOA, TÜBİTAK and AMAAU internship and travel funds to EST and KB, and University of Virginia College of Arts and Sciences research funds to AE.

Data Availability No datasets were generated or analysed during the current study.

Declarations

Ethics Approval All procedures involving animal experiments were performed in accordance with the National Institute of Health Guide for the Care and Use of Laboratory Animals (2011) and were approved by the Animal Experiments Local Ethics Committee of the Acibadem Mehmet Ali Aydinlar University (ACU-HADYEK 2019/46).

Competing Interests The authors declare no competing interests.

References

1. Kinney JW, Bemiller SM, Murtishaw AS, Leisgang AM, Salazar AM, Lamb BT (2018) Inflammation as a central mechanism in Alzheimer's disease. Alzheimers Dement (N Y) 4:575–590. https://doi.org/10.1016/j.trci.2018.06.014
2. Flannery PJ, Trushina E (2019) Mitochondrial dynamics and transport in Alzheimer's disease. Mol Cell Neurosci 98:109–120. https://doi.org/10.1016/j.mcn.2019.06.009
3. Zhang Y, Miao Y, Tan J, Chen F, Lei P, Zhang Q (2023) Identification of mitochondrial related signature associated with immune microenvironment in Alzheimer's disease. J Transl Med 21(1):458. https://doi.org/10.1186/s12967-023-04254-9
4. Kerr JS, Adriaanse BA, Greig NH, Mattson MP, Cader MZ, Bohr VA, Fang EF (2017) Mitophagy and Alzheimer's disease: cellular and molecular mechanisms. Trends Neurosci 40(3):151–166. https://doi.org/10.1016/j.tins.2017.01.002
5. Castellani RJ, Hirai K, Aliev G, Drew KL, Nunomura A, Takeda A, Cash AD, Obrenovich ME et al (2002) Role of mitochondrial dysfunction in Alzheimer's disease. J Neurosci Res 70(3):357–360. https://doi.org/10.1002/jnr.10389
6. Baloyannis SJ (2006) Mitochondrial alterations in Alzheimer's disease. J Alzheimers Dis 9(2):119–126. https://doi.org/10.3233/jad-2006-9204
7. Baloyannis SJ (2011) Mitochondria are related to synaptic pathology in Alzheimer's disease. Int J Alzheimer S Dis 2011(1):305395. https://doi.org/10.4061/2011/305395
8. Mairet-Coello G, Courchet J, Pieraut S, Courchet V, Maximov A, Polleux F (2013) The CAMKK2-AMPK kinase pathway mediates the synaptotoxic effects of Aβ oligomers through Tau phosphorylation. Neuron 78(1):94–108. https://doi.org/10.1016/j.neuron.2013.02.003
9. Fang EF, Hou Y, Palikaras K, Adriaanse BA, Kerr JS, Yang B, Lautrup S, Hasan-Olive MM et al (2019) Mitophagy inhibits amyloid-β and tau pathology and reverses cognitive deficits in models of Alzheimer's disease. Nat Neurosci 22(3):401–412. https://doi.org/10.1038/s41593-018-0332-9
10. Haun F, Nakamura T, Lipton SA (2013) Dysfunctional mitochondrial dynamics in the pathophysiology of neurodegenerative diseases. J Cell Death 6:JCD.S10847. https://doi.org/10.4137/JCD.S10847
11. Berbusse GW, Woods LC, Vohra BPS, Naylor K (2016) Mitochondrial dynamics decrease prior to axon degeneration ınduced by vincristine and are partially rescued by overexpressed cytNmnat1. Front Cell Neurosci 10:179. https://doi.org/10.3389/fncel.2016.00179
12. Spuch C, Ortolano S, Navarro C (2012) New insights in the amyloid-beta interaction with mitochondria. J Aging Res 2012:324968. https://doi.org/10.1155/2012/324968
13. Baloyannis, SJ (2019) Mitochondria and Alzheimer's disease: an electron microscopy study. In: Larrivee D (ed) Redirecting Alzheimer strategy - Tracing memory loss to self pathology. IntechOpen. https://doi.org/10.5772/intechopen.84881
14. Baloyannis SJ, Costa V, Michmizos D (2004) Mitochondrial alterations in Alzheimer's disease. Am J Alzheimers Dis Other Demen 19(2):89–93. https://doi.org/10.1177/153331750401900205
15. Skalka GL, Tsakovska M, Murphy DJ (2024) Kinase signalling adaptation supports dysfunctional mitochondria in disease. Front Mol Biosci 11:1354682. https://doi.org/10.3389/fmolb.2024.1354682
16. Lin MT, Beal MF (2006) Mitochondrial dysfunction and oxidative stress in neurodegenerative diseases. Nature 443(7113):787–795. https://doi.org/10.1038/nature05292
17. Cenini G, Voos W (2019) Mitochondria as potential targets in Alzheimer disease therapy: an update. Front Pharmacol 10:902. https://doi.org/10.3389/fphar.2019.00902
18. Cai Q, Tammineni P (2016) Alterations in mitochondrial quality control in Alzheimer's disease. Front Cell Neurosci 10:24. https://doi.org/10.3389/fncel.2016.00024
19. Hirai K, Aliev G, Nunomura A, Fujioka H, Russell RL, Atwood CS, Johnson AB, Kress Y et al (2001) Mitochondrial abnormalities in Alzheimer's disease. J Neurosci 21(9):3017–3023. https://doi.org/10.1523/jneurosci.21-09-03017.2001
20. Sebastián D, Zorzano A (2018) Mitochondrial dynamics and metabolic homeostasis. Curr Opin Physio 3:34–40. https://doi.org/10.1016/j.cophys.2018.02.006
21. Reiss AB, Gulkarov S, Jacob B, Srivastava A, Pinkhasov A, Gomolin IH, Stecker MM, Wisniewski T et al (2024) Mitochondria in Alzheimer's disease pathogenesis. Life 14(2):196. https://doi.org/10.3390/life14020196
22. Scorrano L (2013) Keeping mitochondria in shape: a matter of life and death. Eur J Clin Invest 43(8):886–893. https://doi.org/10.1111/eci.12135
23. Liu YJ, McIntyre RL, Janssens GE, Houtkooper RH (2020) Mitochondrial fission and fusion: a dynamic role in aging and potential target for age-related disease. Mech Ageing Dev 186:111212. https://doi.org/10.1016/j.mad.2020.111212
24. Giacomello M, Pellegrini L (2016) The coming of age of the mitochondria-ER contact: a matter of thickness. Cell Death Differ 23(9):1417–1427. https://doi.org/10.1038/cdd.2016.52
25. Sassano ML, Felipe-Abrio B, Agostinis P (2022) ER-mitochondria contact sites; a multifaceted factory for Ca2+ signaling and lipid transport. Front Cell Dev Biol 10:988014. https://doi.org/10.3389/fcell.2022.988014
26. Aoyama-Ishiwatari S, Hirabayashi Y (2021) Endoplasmic reticulum–mitochondria contact sites—emerging ıntracellular signaling hubs. Front Cell Dev Biol 9:653828. https://doi.org/10.3389/fcell.2021.653828
27. Wang W, Zhao F, Ma X, Perry G, Zhu X (2020) Mitochondria dysfunction in the pathogenesis of Alzheimer's disease: recent advances. Mol Neurodegener 15(1):30. https://doi.org/10.1186/s13024-020-00376-6
28. Wang L, Guo L, Lu L, Sun H, Shao M, Beck SJ, Li L, Ramachandran J et al (2016) Synaptosomal mitochondrial dysfunction in 5xFAD mouse model of Alzheimer's disease. PLoS ONE 11(3):e0150441. https://doi.org/10.1371/journal.pone.0150441
29. Sharma N, Banerjee R, Davis RL (2023) Early mitochondrial defects in the 5xFAD mouse model of Alzheimer's disease. J Alzheimers Dis 91(4):1323–1338. https://doi.org/10.3233/jad-220884
30. Wang X, Su B, Lee HG, Li X, Perry G, Smith MA, Zhu X (2009) Impaired balance of mitochondrial fission and fusion in Alzheimer's disease. J Neurosci 29(28):9090–9103. https://doi.org/10.1523/jneurosci.1357-09.2009
31. Bell SM, Barnes K, De Marco M, Shaw PJ, Ferraiuolo L, Blackburn DJ, Venneri A, Mortiboys H (2021) Mitochondrial dysfunction in Alzheimer's disease: a biomarker of the future? Biomedicines 9(1):63. https://doi.org/10.3390/biomedicines9010063
32. Delbarba A, Abate G, Prandelli C, Marziano M, Buizza L, Arce Varas N, Novelli A, Cuetos F et al (2016) Mitochondrial alterations in peripheral mononuclear blood cells from Alzheimer's disease and mild cognitive ımpairment patients. Oxid Med Cell Longev 2016:5923938. https://doi.org/10.1155/2016/5923938
33. Silaidos C, Pilatus U, Grewal R, Matura S, Lienerth B, Pantel J, Eckert GP (2018) Sex-associated differences in mitochondrial function in human peripheral blood mononuclear cells (PBMCs)

and brain. Biol Sex Differ 9(1):34. https://doi.org/10.1186/s13293-018-0193-7
34. Leuner K, Schulz K, Schütt T, Pantel J, Prvulovic D, Rhein V, Savaskan E, Czech C et al (2012) Peripheral mitochondrial dysfunction in Alzheimer's disease: focus on lymphocytes. Mol Neurobiol 46(1):194–204. https://doi.org/10.1007/s12035-012-8300-y
35. Ruiz-Pérez G, de Martín R, Esteban S, Marqués S, Aparicio N, Grande MT, Benito-Cuesta I, Martínez-Relimpio AM et al (2021) Potentiation of amyloid beta phagocytosis and amelioration of synaptic dysfunction upon FAAH deletion in a mouse model of Alzheimer's disease. J Neuroinflammation 18(1):223. https://doi.org/10.1186/s12974-021-02276-y
36. AlzForum 5xFAD (B6SJL). https://www.alzforum.org/research-models/5xfad-b6sjl. Accessed 14 May 2015
37. Wilcock DM, Gordon MN, Morgan D (2006) Quantification of cerebral amyloid angiopathy and parenchymal amyloid plaques with Congo red histochemical stain. Nat Protoc 1(3):1591–1595. https://doi.org/10.1038/nprot.2006.277
38. Erisir A, Dreusicke M (2005) Quantitative morphology and postsynaptic targets of thalamocortical axons in critical period and adult ferret visual cortex. J Comp Neurol 485(1):11–31. https://doi.org/10.1002/cne.20507
39. Joslin J (2009) Blood collection techniques in exotic small mammals. J Exot Pet Med 18:117–139. https://doi.org/10.1053/j.jepm.2009.04.002
40. Amos D, Pool P (1976) HLA typing" in Manual of clinical ımmunology. In: Rose NR, and Friedman, H. (ed). American Society for Microbiology, Washington, DC
41. Puleston D (2015) Detection of mitochondrial mass, damage, and reactive oxygen species by flow cytometry. Cold Spring Harb Protoc 2015(9):pdb.prot086298. https://doi.org/10.1101/pdb.prot086298
42. Monteiro LB, Davanzo GG, de Aguiar CF, Moraes-Vieira PMM (2020) Using flow cytometry for mitochondrial assays. MethodsX 7:100938. https://doi.org/10.1016/j.mex.2020.100938
43. Cottet-Rousselle C, Ronot X, Leverve X, Mayol JF (2011) Cytometric assessment of mitochondria using fluorescent probes. Cytometry A 79(6):405–425. https://doi.org/10.1002/cyto.a.21061
44. Santos RX, Correia SC, Wang X, Perry G, Smith MA, Moreira PI, Zhu X (2010) A synergistic dysfunction of mitochondrial fission/fusion dynamics and mitophagy in Alzheimer's disease. J Alzheimers Dis 20(Suppl 2):S401-412. https://doi.org/10.3233/jad-2010-100666
45. Calkins MJ, Manczak M, Mao P, Shirendeb U, Reddy PH (2011) Impaired mitochondrial biogenesis, defective axonal transport of mitochondria, abnormal mitochondrial dynamics and synaptic degeneration in a mouse model of Alzheimer's disease. Hum Mol Genet 20(23):4515–4529. https://doi.org/10.1093/hmg/ddr381
46. Wang W, Yin J, Ma X, Zhao F, Siedlak SL, Wang Z, Torres S, Fujioka H et al (2017) Inhibition of mitochondrial fragmentation protects against Alzheimer's disease in rodent model. Hum Mol Genet 26(21):4118–4131. https://doi.org/10.1093/hmg/ddx299
47. Mishra P, Carelli V, Manfredi G, Chan DC (2014) Proteolytic cleavage of Opa1 stimulates mitochondrial inner membrane fusion and couples fusion to oxidative phosphorylation. Cell Metab 19(4):630–641. https://doi.org/10.1016/j.cmet.2014.03.011
48. Liesa M, Palacín M, Zorzano A (2009) Mitochondrial dynamics in mammalian health and disease. Physiol Rev 89(3):799–845. https://doi.org/10.1152/physrev.00030.2008
49. DuBoff B, Götz J, Feany MB (2012) Tau promotes neurodegeneration via DRP1 mislocalization in vivo. Neuron 75(4):618–632. https://doi.org/10.1016/j.neuron.2012.06.026
50. Zhang L, Trushin S, Christensen TA, Bachmeier BV, Gateno B, Schroeder A, Yao J, Itoh K et al (2016) Altered brain energetics induces mitochondrial fission arrest in Alzheimer's Disease. Sci Rep 6:18725. https://doi.org/10.1038/srep18725
51. Smith AM, Depp C, Ryan BJ, Johnston GI, Alegre-Abarrategui J, Evetts S, Rolinski M, Baig F et al (2018) Mitochondrial dysfunction and increased glycolysis in prodromal and early Parkinson's blood cells. Mov Disord 33(10):1580–1590. https://doi.org/10.1002/mds.104
52. Zhao RZ, Jiang S, Zhang L, Yu ZB (2019) Mitochondrial electron transport chain, ROS generation and uncoupling (review). Int J Mol Med 44(1):3–15. https://doi.org/10.3892/ijmm.2019.4188
53. Grasmick KA, Hu H, Hone EA, Farooqi I, Rellick SL, Simpkins JW, Ren X (2018) Uncoupling of the electron transport chain compromises mitochondrial oxidative phosphorylation and exacerbates stroke outcomes. J Neuroinfect Dis 9(4):283. https://doi.org/10.4172/2314-7326.1000283
54. Rimal S, Tantray I, Li Y, Pal Khaket T, Li Y, Bhurtel S, Li W, Zeng C et al (2023) Reverse electron transfer is activated during aging and contributes to aging and age-related disease. EMBO Rep 24(4):e55548. https://doi.org/10.15252/embr.202255548
55. Scialò F, Fernández-Ayala DJ, Sanz A (2017) Role of mitochondrial reverse electron transport in ROS signaling: potential roles in health and disease. Front Physiol 8:428. https://doi.org/10.3389/fphys.2017.00428
56. Trushina E (2019) Alzheimer's disease mechanisms in peripheral cells: promises and challenges. Alzheimers Dement (N Y) 5:652–660. https://doi.org/10.1016/j.trci.2019.06.008
57. Yousaf A, Deeba F, Younis S, Iqbal N, Aslam F (2022) Starrıng role of mıtochondrıal ımpaırment ın Alzheımer's dısease neuropathology. J Mıcrobıol Mole Genet 3:77–104. https://doi.org/10.52700/jmmg.v3i2.70
58. Calvo-Rodriguez M, Kharitonova EK, Snyder AC, Hou SS, Sanchez-Mico MV, Das S, Fan Z, Shirani H et al (2024) Real-time imaging of mitochondrial redox reveals increased mitochondrial oxidative stress associated with amyloid β aggregates in vivo in a mouse model of Alzheimer's disease. Mol Neurodegener 19(1):6. https://doi.org/10.1186/s13024-024-00702-2
59. Villeda SA, Luo J, Mosher KI, Zou B, Britschgi M, Bieri G, Stan TM, Fainberg N et al (2011) The ageing systemic milieu negatively regulates neurogenesis and cognitive function. Nature 477(7362):90–94. https://doi.org/10.1038/nature10357
60. Li C, Stebbins RC, Noppert GA, Carney CX, Liu C, Sapp ARM, Watson EJ, Aiello AE (2024) Peripheral immune function and Alzheimer's disease: a living systematic review and critical appraisal. Mol Psychiatry 29(6):1895–1905. https://doi.org/10.1038/s41380-023-02355-x
61. Morris G, Berk M, Maes M, Puri BK (2019) Could Alzheimer's disease originate in the periphery and ıf so how so? Mol Neurobiol 56(1):406–434. https://doi.org/10.1007/s12035-018-1092-y
62. Bettcher BM, Tansey MG, Dorothée G, Heneka MT (2021) Peripheral and central immune system crosstalk in Alzheimer disease — a research prospectus. Nat Rev Neurol 17(11):689–701. https://doi.org/10.1038/s41582-021-00549-x
63. Leal NS, Martins LM (2021) Mind the gap: mitochondria and the endoplasmic reticulum in neurodegenerative diseases. Biomedicines 9(2):227
64. Jörg M, Plehn JE, Friedland K, Müller WE (2021) Mitochondrial dysfunction as a causative factor in Alzheimer's disease-spectrum disorders: lymphocytes as a window to the brain. Curr Alzheimer Res 18(10):733–752. https://doi.org/10.2174/1567205018666211208141512
65. Manczak M, Calkins MJ, Reddy PH (2011) Impaired mitochondrial dynamics and abnormal interaction of amyloid beta with mitochondrial protein Drp1 in neurons from patients with Alzheimer's disease: implications for neuronal damage. Hum Mol Genet 20(13):2495–2509. https://doi.org/10.1093/hmg/ddr139

66. Bhatti JS, Kaur S, Mishra J, Dibbanti H, Singh A, Reddy AP, Bhatti GK (1869) Reddy PH (2023) Targeting dynamin-related protein-1 as a potential therapeutic approach for mitochondrial dysfunction in Alzheimer's disease. Biochim Biophys Acta Mol Basis Dis 7:166798. https://doi.org/10.1016/j.bbadis.2023.166798
67. Kim DI, Lee KH, Gabr AA, Choi GE, Kim JS, Ko SH (1863) Han HJ (2016) Aβ-Induced Drp1 phosphorylation through Akt activation promotes excessive mitochondrial fission leading to neuronal apoptosis. Biochim Biophys Acta 11:2820–2834. https://doi.org/10.1016/j.bbamcr.2016.09.003
68. Medala VK, Gollapelli B, Dewanjee S, Ogunmokun G, Kandimalla R, Vallamkondu J (2021) Mitochondrial dysfunction, mitophagy, and role of dynamin-related protein 1 in Alzheimer's disease. J Neurosci Res 99(4):1120–1135. https://doi.org/10.1002/jnr.24781
69. Manczak M, Kandimalla R, Fry D, Sesaki H, Reddy PH (2016) Protective effects of reduced dynamin-related protein 1 against amyloid beta-induced mitochondrial dysfunction and synaptic damage in Alzheimer's disease. Hum Mol Genet 25(23):5148–5166. https://doi.org/10.1093/hmg/ddw330
70. Galluzzi L, Blomgren K, Kroemer G (2009) Mitochondrial membrane permeabilization in neuronal injury. Nat Rev Neurosci 10(7):481–494. https://doi.org/10.1038/nrn2665
71. Zampese E, Fasolato C, Pozzan T, Pizzo P (2011) Presenilin-2 modulation of ER-mitochondria interactions: FAD mutations, mechanisms and pathological consequences. Commun Integr Biol 4(3):357–360. https://doi.org/10.4161/cib.4.3.15160
72. Nelson O, Tu H, Lei T, Bentahir M, de Strooper B, Bezprozvanny I (2007) Familial Alzheimer disease-linked mutations specifically disrupt Ca2+ leak function of presenilin 1. J Clin Invest 117(5):1230–1239. https://doi.org/10.1172/jci30447
73. Correia SC, Perry G (1862) Moreira PI (2016) Mitochondrial traffic jams in Alzheimer's disease - pinpointing the roadblocks. Biochimica et Biophysica Acta (BBA) - Mole Basis Dis 10:1909–1917. https://doi.org/10.1016/j.bbadis.2016.07.010
74. Sathyamurthy VH, Nagarajan Y, Parvathi VD (2024) Mitochondria-Endoplasmic Reticulum Contact Sites (MERCS): a new axis in neuronal degeneration and regeneration. Mol Neurobiol 61(9):6528–6538. https://doi.org/10.1007/s12035-024-03971-6
75. Leal NS, Dentoni G, Schreiner B, Naia L, Piras A, Graff C, Cattaneo A, Meli G et al (2020) Amyloid B-peptide ıncreases mitochondria-endoplasmic reticulum contact altering mitochondrial function and autophagosome formation in Alzheimer's disease-related models. Cells 9(12):2552. https://doi.org/10.3390/cells9122552
76. Molina JA, de Bustos F, Jiménez-Jiménez FJ, Benito-León J, Gasalla T, Ortí-Pareja M, Vela L, Bermejo F et al (1997) Respiratory chain enzyme activities in isolated mitochondria of lymphocytes from patients with Alzheimer's disease. Neurology 48(3):636–638. https://doi.org/10.1212/wnl.48.3.636
77. Casademont J, Miró O, Rodriguez-Santiago B, Viedma P, Blesa R, Cardellach F (2003) Cholinesterase inhibitor rivastigmine enhance the mitochondrial electron transport chain in lymphocytes of patients with Alzheimer's disease. J Neurol Sci 206(1):23–26. https://doi.org/10.1016/s0022-510x(02)00319-2
78. Feldhaus P, Fraga DB, Ghedim FV, De Luca RD, Bruna TD, Heluany M, Matos MP, Ferreira GK et al (2011) Evaluation of respiratory chain activity in lymphocytes of patients with Alzheimer disease. Metab Brain Dis 26(3):229–236. https://doi.org/10.1007/s11011-011-9253-y
79. Mahapatra G, Gao Z, Bateman JR 3rd, Lockhart SN, Bergstrom J, DeWitt AR, Piloso JE, Kramer PA et al (2023) Blood-based bioenergetic profiling reveals differences in mitochondrial function associated with cognitive performance and Alzheimer's disease. Alzheimers Dement 19(4):1466–1478. https://doi.org/10.1002/alz.12731
80. Manczak M, Reddy PH (2012) Abnormal interaction of VDAC1 with amyloid beta and phosphorylated tau causes mitochondrial dysfunction in Alzheimer's disease. Hum Mol Genet 21(23):5131–5146. https://doi.org/10.1093/hmg/dds360
81. Shoshan-Barmatz V, Nahon-Crystal E, Shteinfer-Kuzmine A, Gupta R (2018) VDAC1, mitochondrial dysfunction, and Alzheimer's disease. Pharmacol Res 131:87–101. https://doi.org/10.1016/j.phrs.2018.03.010
82. Pérez-Gracia E, Torrejón-Escribano B, Ferrer I (2008) Dystrophic neurites of senile plaques in Alzheimer's disease are deficient in cytochrome c oxidase. Acta Neuropathol 116(3):261–268. https://doi.org/10.1007/s00401-008-0370-6